UC San Diego
UC San Diego Previously Published Works

Title

New archaeomagnetic direction results from China and their constraints on palaeosecular variation of the geomagnetic field in Eastern Asia

Permalink

https://escholarship.org/uc/item/71s933sz

Journal

Geophysical Journal International, 207(2)

ISSN

0956-540X

Authors

Cai, Shuhui
Tauxe, Lisa
Deng, Chenglong
et al.

Publication Date

2016-11-01

DOI

10.1093/gji/ggw351

Peer reviewed

eScholarship.org Powered by the California Digital Library
University of California

New archaeomagnetic direction result from China and its constraints on paleosecular variation of the geomagnetic field in Eastern Asia

Journal:	*Geophysical Journal International*
Manuscript ID	Draft
Manuscript Type:	Research Paper
Date Submitted by the Author:	n/a
Complete List of Authors:	Cai, Shuhui; Institute of Geology and Geophysics Chinese Academy of Sciences, ; University of California San Diego Scripps Institution of Oceanography, Tauxe, Lisa; Scripps Oceanographic Institution, Deng, Chenglong; State Key Laboratory of Lithospheric Evolution, Institute of Geology and Geophysics, Chinese Academy of Sciences, Qin, Huafeng; Institute of Geology and Geophysics, State Key Laboratory of Lithospheric Evolution Pan, Yongxin; Institute of Geology and Geophysics Chinese Academy of Sciences Jin, Guiyun; Shandong University, School of History and Culture Chen, Xuexiang; Shandong University, School of History and Culture Chen, Wei; The Sichuan Provincial Cultural Relics and Archeology Research Institute Xie, Fei; Hebei Province Institute of Cultural Relics Zhu, Rixiang; Institute of Geology and Geophysics Chinese Academy of Sciences
Keywords:	Archaeomagnetism < GEOMAGNETISM and ELECTROMAGNETISM, Palaeomagnetic secular variation < GEOMAGNETISM and ELECTROMAGNETISM, Palaeomagnetism < GEOMAGNETISM and ELECTROMAGNETISM

SCHOLARONE™
Manuscripts

New archaeomagnetic direction result from China and its constraints on paleosecular variation of the geomagnetic field in Eastern Asia

Shuhui Cai,[1, 2], Lisa Tauxe,[2], Chenglong Deng,[1, 3], Huafeng Qin,[3], Yongxin Pan,[3, 4], Guiyun Jin,[5], Xuexiang Chen,[5], Wei Chen,[6], Fei Xie[7] and Rixiang Zhu[1, 3]

[1] State Key Laboratory of Lithospheric Evolution, Institute of Geology and Geophysics, Chinese Academy of Sciences, Beijing 100029, China Email: caishuhui@mail.iggcas.ac.cn

[2] Scripps Institution of Oceanography, University of California, San Diego, La Jolla, CA 92093-0220, USA

[3] University of Chinese Academy of Sciences, Beijing 100049, China

[4] Key Laboratory of the Earth and Planetary Physics, Institute of Geology and Geophysics, Chinese Academy of Sciences, Beijing 100029, China

[5] School of History and Culture, Shandong University, Jinan 250100, China

[6] The Sichuan Provincial Cultural Relics and Archeology Research Institute, Chengdu 610041, China

[7] Hebei Province Institute of Cultural Relics, Shijiazhuang 050000, China

SUMMARY

We carried out an archaeomagnetic directional study on 38 oriented samples (bricks and baked clays) collected from four archaeological locations at three provinces in China. The ages of our samples, spanning from ~3000 BCE to ~1300 CE, were constrained using a combination of archaeological context, radiocarbon dating and stratigraphic information. Rock magnetic results demonstrate that the main magnetic minerals of the studied samples are magnetite and/or hematite in single domain (SD) and superparamagnetic (SP) states. A total of 20 new reliable archaeodirectional data from 12 independent sites are obtained after thermal demagnetization experiments. These are the first set of archaeodirectional data in China produced since the 1990s. The published data are largely from the past 2 kyr and data from older time periods are rare. Our new data, especially those from period older than 3 ka, fill many gaps of the presently published dataset and will provide strong constraints on paleosecular variation (PSV) of the geomagnetic field in Eastern Asia and on the improvement of global models. In this study, we combine our new data with published ones and the predictions of global models, to discuss the PSV of the geomagnetic field in Eastern Asia over the past 10 kyr.

Key words: archaeomagnetic direction; China; paleosecular variation; Eastern Asia.

1 INTRODUCTION

Paleosecular variation of the geomagnetic field during the Holocene is important for our understanding of the geodynamic mechanisms on time scales from decades to millennia (Amit *et al.* 2011; Aubert *et al.* 2013; Tarduno *et al.* 2015). High-resolution records over the last few millennia are also useful for stratigraphic chronology (Barletta *et al.* 2010; Ólafsdóttir *et al.* 2013) and archaeomagnetic dating (Ben-Yosef *et al.* 2008b; Pavón-Carrasco *et al.* 2011; Ertepinar *et al.* 2016). The establishment and updating of various reference field models, such as CALS10k.1b (Korte *et al.* 2011), pfm9k (Nilsson *et al.* 2014), ARCH3k.1 (Korte *et al.* 2009) and CALS3k.4 (Korte & Constable 2011), ultimately rely on having a large quantity of reliable data from around the globe in the Holocene. In the past few years, a number of PSV curves from sediments spanning the Holocene in Eastern Asia were published (Ali *et al.* 1999; Hyodo *et al.* 1999; Frank 2007; Yang *et al.* 2009, 2012, 2016; Zheng *et al.* 2014). However, data from archaeological materials or lava flows, which can record data points with high precision and high temporal resolution, are sparse. The archaeomagnetic directions for China compiled in the GEOMAGIA50 database (https://geomagia.ucsd.edu, Brown *et al.* 2015) were mainly published in the 1980s (Wei *et al.* 1981, 1983, 1984; Batt *et al.* 1998). A total of 80 directions are in the database and only 29 of them have both declination and inclination, while the other 51 include only inclinations. Data from Korea were all published by Yu *et al.* (2010) and no publications are available before that. The Japanese data are relatively abundant and have been published between 1967 and 2008 (all the references can be found in the GEOMAGIA50 database). But even in this most robust of the eastern Asian data sets, most of the data points are from the past 1.5 kyr and older data are rare. In this study, we carried out an archaeomagnetic directional study on oriented samples collected from four archaeological locations in three provinces of China and two of them are from a time period older than 3 ka, which will supply important constraints on the PSV of the geomagnetic field in Eastern Asia.

2 SAMPLING BACKGROUND

The samples in this study were collected from four archaeological locations in three provinces in China, which are Baojiaying (BJY) in Hebei, Daxinzhuang (DXZ) and Shuangwangcheng (SWC) in Shandong and Liujiazhai (LJZ) in Sichuan (Fig. 1a).

The BJY site, located in Longhua county, Chengde city, was a major kiln factory that started during the Liao-Jin dynasty (907-1125 AD) and terminated in the Yuan dynasty (1271-1368 AD). The kilns excavated at this site are usually well preserved probably because of the short period of activity. We collected six oriented samples including bricks and burnt clay from the edge of one of those kilns, which were fired during the Yuan dynasty (Fig. 1b). Of these, only two bricks (BJY2 and BJY5) survived as the others broke because of the fragile texture.

The DXZ site, located at Jinan, Shandong province, is a large living site dated to late Shang dynasty (1300-1000 BCE), from which a large number of building bases, hearths and graves were unearthed. We collected oriented burnt clays from four different firing units: DXZ1, (hearth; Fig. 1c), DXZ3-DXZ8 (round kiln-like structure), DXZ9-DXZ11 (channel of a kiln) and DXZ12-DXZ15 (two strips of burnt clay).

The SWC site is located in Shouguang, Shandong province, which is near the Bohai Sea. This site used to be a huge area for salt manufacturing with ages ranging from the Shang (1600-1000 BCE) to the Song-Yuan (960-1368 AD) dynasty. A number of hearths whose original purpose was for boiling brine were excavated and we collected three oriented samples from one hearth dated to Song-Yuan dynasty (Fig. 1d).

The LJZ site, located in Jinchuan, Sichuan province, belongs to the late Neolithic period with an age of approximately 3000 BCE (Fig. 1e). Various artifacts including pottery kilns, hearths, ash pits and house vestiges were uncovered at this site. We collected oriented samples from seven kilns (Y2-Y8). Here we treat each kiln as a separate cooling unit and to avoid any confusion, we use the kiln names defined by the archaeologists to name our samples. For example, in Y32-01, 'Y3' is the kiln name, '2' is the sample name and '01' is the specimen name.

We employed three kinds of orientation methods during sample collection. For well-consolidated baked clay (Fig. 1d), we shaved a horizontal plane on the surface with a non-magnetic knife and a bubble level, marking the north direction with a magnetic compass. In those cases where it was difficult to shave a horizontal surface on the samples, we made a plane with non-magnetic plaster and marked the north direction on it (Fig. 1c and e) and then transferred the direction to each specimen during processing. For the hard samples such as rocks beside the kiln in LJZ (Y21 and Y31), we measured the attitude of the samples with a magnetic compass and then corrected the results during data processing. All the oriented block samples were cut into cubic specimens (2 cm×2 cm×2 cm) in the laboratory.

Dating of the samples from BJY, DXZ and SWC relies on archaeological context. Because radiocarbon materials (charcoals and animal bones) and clear cultural layers are available in LJZ site, we adopted various dating techniques, including radiocarbon analysis, stratigraphic information as well as archaeological background, to determine the ages of the kilns. The detailed description about dating can be found in Cai *et al.* (2015). Here we include only the dating results used in this study.

In total, 48 oriented samples (6, 15, 3 and 24 from BJY, DXZ, SWC and LJZ, respectively) were collected in this study, but only 38 (2, 15, 3 and 18 from BJY, DXZ, SWC and LJZ, respectively) of them were successfully processed and underwent a thermal demagnetization experiment. The sample information including ages and dating methods of each unit are listed in Table 1.

3 EXPERIMENTAL TECHNIQUES

3.1 Rock magnetic experiments

We carried out rock magnetic experiments including hysteresis loops, first order reversal curves (FORCs) and variation of susceptibility versus temperature (χ-T) to determine the magnetic mineralogy of the studied samples. Hysteresis loops and FORCs were measured with the MicroMag 3900 VSM in the Paleomagnetism and Geochronology Laboratory (PGL) at the Institute of Geology and Geophysics, Chinese Academy of Sciences (IGGCAS). χ-T curves were measured on the Kappabridge MFK1-FA system (made by AGICO Ltd., Brno, Czech Republic) in air environment at the frequency of 967 Hz. Since alteration temperature of archaeological samples during heating can be used for estimating the original firing temperature of the artifacts, we measured step-wise χ-T curves (300ºC, 500ºC, 600ºC and 700ºC) to determine the alteration temperature. The rock magnetic characteristics will contribute to understanding demagnetizing behaviors of the samples.

3.2 Thermal demagnetization methods

Samples collected as blocks were processed into cubic specimens (2 cm×2 cm×2 cm). We conducted step-wise thermal demagnetization experiments on these specimens to separate the characteristic remanent magnetization (ChRM). The demagnetizing procedures were carried out on the ASC-MMTD48 thermal demagnetizer oven with a residual field of less than 10 nT in the cooling chamber. Step intervals vary from 50ºC to 20ºC, larger at low temperatures and smaller at high temperatures. We measured the natural remanent magnetization (NRM) and remanence remaining after each step with a 2G 755 SQUID magnetometer. The demagnetizing procedure terminates when the remanence drops to less than 10% of the NRM. All the procedures were conducted in the shielded room with residual field less than 300 nT at PGL.

4 RESULTS

4.1 Rock magnetism

Representative hysteresis loops and FORCs are shown in Fig. 2. Generally, the coercivities (B_cs) of the samples are ~10 mT (Fig. 2b-f), indicating the dominance of soft magnetic minerals. An exception is BJY2 (Fig. 2a), which is still unsaturated at the high field of 2 T and with a minimum coercivity of 164 mT, demonstrating the existence of hard magnetic carriers, such as hematite. The shapes of the FORCs (Fig. 2g-i) allow us to explain the grain sizes of the magnetic particles as mixtures of SD and SP, some of which have relatively strong interactions between particles (Fig. 2i).

The χ-T curves shown in Fig. 3 can give a rough estimation of the Curie/Neél temperature (T_c/T_N) of magnetic minerals in the sample and also help detect the mineral alterations during heating. The representative χ-T curves show that T_c/T_Ns of the samples are usually over 600ºC (Fig. 3d, l, p) while that of DXZ1 is ~580ºC (Fig.

3h). The latter indicates magnetite as the main magnetic carrier. However, the values in excess of 600ºC, could point to a hematitic mineralogy (Tauxe *et al.* 2010). Yet hematite is not consistent with the lack of high coercivity components in the hysteresis results (SWC2 and Y82). Combining all the rock magnetic characteristics, we may attribute the high T_c/T_Ns to the presence of fine-grained hematite (in the SP state, for example); this interpretation will be further supported by the thermal demagnetization results.

The step-wise χ-T curves of BJY2 (Fig. 3a-d) are reversible at each temperature until 700ºC, illustrating that no alteration happens during heating and the original firing temperature may be over 700ºC. The step-wise χ-T curves of DXZ1 (Fig. 3e-h) show that slight alteration starts at 500ºC and alteration becomes significant over 600ºC, from which we can infer that the original firing temperature of this sample was likely to be around 500ºC. Alteration at 700ºC is apparent for SWC2 (Fig. 3i-l) and Y82 (Fig. 3m-p), indicating that the alteration may start at any temperature over 600ºC. That is to say, these samples were originally fired to a temperature of above 600ºC.

From the representative diagrams of orthogonal projections (Zijderveld 1967) for successful specimens (Fig. 4), we see that some of the specimens (BJY2-02 and SWC2-10) are totally demagnetized by around 620ºC (Fig. 4a and d). Both of their χ-T curves suggested the existence of hematite but the B_cs of BJY2 and SWC2 are ~164 mT and ~12 mT respectively, from which we can infer that these samples have hematite with different grain sizes, where the former is coarser and the latter is finer

(Banerjee 1971; Jiang *et al.* 2014). The remanence of other samples decreases to less than 10% of the NRM around 450-500ºC (Fig. 4b and c). This is consistent with the conclusion drawn from the step-wise χ-T curves that the remanences of these samples are carried by partial thermal remanent magnetization (pTRM). In this case, the totally demagnetized temperature is mainly dependent on the original firing temperature rather than the T_c/T_N of the magnetic carriers. Other samples are totally demagnetized by around 540-560ºC (Fig. 4e and f). But the χ-T curve of Y82 (Fig. 3p) indicates the existence of hematite while the hysteresis characteristics do not show any high coercivity component (Fig. 2f). This possibly can be explained by an assumption that these samples contain fine-grained hematite in the SP state, as this fraction would not contribute to the remanence.

In summary, the rock magnetic results demonstrate that the main magnetic minerals of the studied samples are magnetite and/or hematite in SD and SP state. The original firing temperatures of our samples varied from ~500ºC to at least 700ºC, (higher values can not be determined by the χ-T curves), indicating that the remanence of our samples is carried by either total TRM (as BJY2) or pTRM (as DXZ1). This makes us optimistic that the geomagnetic directions recorded by the studied samples represent the ones while they were last fired.

4.2 Archaeomagnetic directions

We calculated the direction of ChRM for each specimen (green lines in Fig. 4) following the method of principal component analysis (Kirschvink 1980). When analyzing the thermal demagnetization data, we followed three basic criteria: 1) the deviation angle from the origin (DANG of Tauxe & Staudigel (2004)) must be less than 6°; 2) the maximum angle of deviation (MAD of Kirschvink (1980)) is less than 6°; and 3) the number of data points used for statistics is no less than four. In total, 188 out of 236 specimens passed these selection criteria. However, a few of the "successful" specimens record abnormal directions (Table S1); these are interpreted as having been incorrectly oriented during sampling (DXZ15) or processing (BJY5-02 and BJY5-04) as these specimens have remarkably different directions from sister specimens from the same cooling unit (e.g. DXZ3-03 and DXZ5-15 in Table S1), we consider these few "deviant" specimens to be outliers. In order to avoid contaminating an otherwise excellent result, we exclude those specimens discussed above from further statistics although they passed the selection criteria. Finally, 171 specimens are considered to record reliable geomagnetic field directions; hence, we have a success rate of ~72%. All the results of specimens passing the selection criteria are listed in Table S1, with all the accepted specimens marked with a flag of 'g' while those excluded from further analysis are marked with 'b'.

Fisher statistics (Fisher 1953) were employed when calculating the mean directions of samples and sites. We treat samples from the same archaeological unit (a hearth or a kiln), which are supposed to be the same age, as a paleomagnetic site. The locations of BJY and SWC both have only one cooling unit, which can also be treated as a site. However, samples from DXZ belong to four different cooling units (DXZ1, DXZ3-DXZ8, DXZ9-DXZ11, DXZ12-DXZ15), and we calculate the site mean directions separately. Samples from LJZ belong to seven independent kilns and each kiln is treated as a site. Since some of the block samples were very fragile, and were small, so only few standard specimens are available for them. However, for those specimens that behaved well during thermal demagnetization and were consistent with each other, it is not reasonable to reject them just because the number is not enough for sample average, especially when we are certain they belong to the same age. Therefore, we calculate the Fisher mean of all the specimens from each kiln to get site mean instead of sample mean from each individually oriented sample.

We converted each site mean direction into virtual geomagnetic poles (VGPs). The statistical results for sample and site level are listed in Table 1. On sample level, only those with at least three accepted specimens and the 95% confidence limit (α_{95}) less than 10° (the α_{95}s of our samples are all less than 8) are accepted. The samples with α_{95} values over 10° (DXZ2 and Y21) are marked with '*' in Table 1 and not included for either statistics of site mean or VGP calculation even though the individual specimens are acceptable. In total, 12 independent site means (1, 4, 1 and 6 from BJY, DXZ, SWC and LJZ, respectively) from 20 reliable sample means were obtained in this study.

5 DISCUSSION

5.1 Compilation of the geomagnetic directions over the last 10 kyr in Eastern Asia

In Fig. 5, we compare our 12 new site mean directions with the published data from

China, Japan and Korea as well as with predictions for a location at the center of China (35°N, 105°E) from the global models (CALS10k.1b (Korte *et al.* 2011), pfm9k (Nilsson *et al.* 2014), ARCH3k.1 (Korte *et al.* 2009) and CALS3k.4 (Korte & Constable 2011). The published data are available in the GEOMAGIA50 database (Brown *et al.* 2015). Only those sites with $\alpha_{95} \leq 10°$ and $\sigma_{age} \leq 600$ yrs are included in Fig. 5. For the published data in China, we include only those with full-scale directions (both declination and inclination). All the published data adopted in this study are listed in Table S2. In order to exclude deviations caused by different latitudes, all the new and published data are relocated to the center of China (35°N, 105°E) following the conversion via VGP method (Noel & Batt 1990). The relocated directions of new and published data can be found in Table 1 and Table S2 respectively.

The declinations of our new data from LJZ dated to ~3000 BCE deviate eastward from both the CALS10k.1b and pfm9k models while the inclinations lie between these two models. A decrease of paleointensity with extreme low value less than 30 ZAm^2 around this age was reported by Cai *et al.* (2015). However, the directional data do not show a significant anomaly apart from the slight eastward deviation of the declinations. There are two possible explanations: one is the geomagnetic intensity anomaly at ~3000 BCE is not associated with a directional change, which is thought to be possible by numerical simulation (Brown & Korte 2016); the other scenario is that we have not captured the large directional anomaly because of either limited temporal and spatial data distribution or insufficient age precision. Additional reliable data from this period are necessary to resolve this issue.

Directions of the four sites in DXZ can be divided into two groups (Fig. 5): DXZ1 (Dec/Inc: 347.4°/56.9°) and DXZ3-8 (Dec/Inc: 345.4°/60.1°), with a combined mean of Dec/Inc: 346.6/58.5, and DXZ9-11 (Dec/Inc: 2.8°/52.4°) and DXZ14 (Dec/Inc: 359.7°/50.0°), with a combined mean of Dec/Inc: 1.2/51.2. This interpretation implies that these archaeological units belong to two different periods although they share the same archaeological age of late Shang dynasty (1300-1000 BCE). Further constraints on relative ages are unfortunately not available. In any case, these four sites provide us with directional information of the field between 1300-1000 BCE and the average of them fit well with the pfm9k model. The results of SWC and BJY are consistent with both the previous data and all of the models, demonstrating their reliability.

Most of the previous data in Eastern Asia have ages concentrated in the past 2 kyr and data from older time period are sparse, which makes our new data, especially those from LJZ and DXZ, significant.

5.2 Paleosecular variation of the geomagnetic field

As shown in Fig. 5, the declination of the geomagnetic field in Eastern Asia varies between 30°W and 20°E while the inclinations range from 30° to 70° over the past 10 kyr. It seems that both the geomagnetic declination and inclination before ~3 ka have limited variations (except the abnormal inclination around 6500 BCE recorded by a single point in the Japanese data). In contrast, at around 300 BCE there is a remarkable sequence of westward drift of the declinations accompanied by shallow inclinations recorded by the Chinese published data. Perhaps because of the rapid directional shift, there is little agreement among different datasets and the global models as the latter are heavily smoothed. For example, the Korean data (Yu *et al.* 2010) have similar shallow inclinations as seen in the Chinese data, but the feature is much younger (~300 CE) in Korea than in China (~300 BCE). Also the Koren inclination anomaly is not accompanied by a declination change but the Chinese feature is seen in both declination and inclination. Moreover, only one of the models (ARCH3k.1) predicts the Chinese inclination anomaly at ~300 BCE and only two predict the declination shift (pfm9k and CALS3k.4). Unfortunately, our new data do not cover this period and no published Japanese data are available from around this age. Therefore, further study is needed to resolve this issue.

The picture improves for the last 1.5 kyr during which the PSV of the geomagnetic field in Eastern Asia is well constrained owing to the abundant published data. The declinations start from a slight eastward deviation at ~500 CE and drift to the west until ~1000 CE, and then recover to the east at ~1500 CE and switch to the west again afterward. The inclinations follow a sinusoidal variation over the past 1.5 kyr, with the steepest directions occurring between 500-1000 CE and a shallowest at ~1500 CE.

In order to further track the directional variation of the geomagnetic field, we calculate Fisher means of the Chinese data and all the Eastern Asian data in Fig. 5 with a time window of 100 years (except that we did not average data point of 100

BCE with other data because it is significantly different from the other directions). These averages are plotted on the declination-inclination (D-I) projection plots in Fig. 6. The average age in each time window is used as the new age. The new and published data are calculated separately for China and jointly for Eastern Asia. The Fisher means of the new data in this study are marked with color dots in Fig. 6a and Fig. 6c (red/cyan/purple/blue: DXZ/LJZ/SWC/BJY). The Chinese data show a general westward movement of the geomagnetic field direction prior to 1000 BCE. Between 1000 BCE and 0 the directions trace a counterclockwise loop, and this pattern continues between 0-1500 CE. When considering PSV of the field in Eastern Asia, it is controlled by the Japanese data before 4500 BCE and by the Chinese data between 4500-1000 BCE, generally following a clockwise motion. Since no data from Japan are available between 1000 BCE-0, the path is mainly controlled by the Chinese data and modified by a few Korean data points, showing a counterclockwise movement generally.

A more detailed record is available after 0 because of the abundance of data. The field moves westward first until ~800 CE, followed by a recovery to the east until ~1500 CE and then back to the west again. Generally, the field in Eastern Asia drifts more to the west than east during the past 10 kyr, which is coincident with the numerical simulation results of Amit *et al.* (2011).

Combining variations of declination and inclination versus age (Fig. 5), we can recognize a few time points/periods when the field changes its sense of motion:

~6500 BCE, ~4000 BCE, ~3000 BCE, ~900-600 BCE, ~300 BCE-0, ~300 CE, ~600-1000 CE and ~1500 CE. Some of them are synchronous with or close to the maxima (~4000 BCE, ~500 CE) and minima (~3000 BCE, ~100 BCE) of the paleointensity in Eastern Asia (Cai *et al.* 2014, 2015), indicating full-vector variations of the field during these periods. Several archaeomagnetic jerks around 800 BCE, 200 CE, 800 CE and 1400 CE were reported in Europe (Gallet *et al.* 2003). As discussed in Yu *et al.* (2010), all of them are recorded in Eastern Asia at similar times but the Eastern Asian data record more field changes. However, it is necessary to mention that these features depend strongly on the precision and resolution of the data, especially the dating. We would like to say it is important to get more reliable data with well constrained ages before we reach unambiguous conclusions.

Based on the Eastern Asian data from Fig. 6 as well as the modern field data at the center of China (35°N, 105°E) from the gufm1 model between 1590-1990 CE (Jackson *et al.* 2000) and the IGRF model between 1990-2010 CE (Finlay *et al.* 2010), we calculated the PSV rate, expressed as the angular variation per year, of the geomagnetic field during the past 10 kyr (Fig. 7). The average rate (red solid circle) is calculated by the angular difference divided by the time interval between two average ages while the lower boundary of the average rate (blue square) is calculated by the same angular difference divided by maximum time interval after considering age uncertainties. The average variation rate is very low between ~6000-2000 BCE (<0.01°/year), followed by an increase after that which reaches a maximum between

500 BCE-0 (>0.2°/year), and fluctuates afterward. The average PSV rate is generally less than 0.15°/year during the past 10 kyr, which is consistent with the variation rate of the modern field (insert in Fig. 7). However, the average variation rate between 500 BCE-0 (with a maximum of ~0.28°/year) is much higher than any observational variation of the modern field in this area. Even the lower boundary, which is the minimum estimation, of the PSV rate shows a notable increase during this period. It is necessary to mention that the data between 500 BCE-0 have undesirable coherence in Eastern Asia and thus the PSV rates during this period should be treated with caution. The calculated variation rates depend on both data precision and time resolution, which will be updated by new reliable data in the future. The discussions in this study are based on our best knowledge at present. The directional variation of the field in Eastern Asia is generally consistent with the paleointensity variation in this area, which is relatively low and with limited variation before ~2000 BCE and increases sharply after then and keeps staying at relatively high values with large fluctuations afterward (Cai *et al.* 2014, 2015). Our new data and compilations of the published data as well as discussions in this study will provide context for numerical modeling in the future.

6 CONCLUSIONS

We present 20 (2, 10, 2 and 6 from BJY, DXZ, SWC and LJZ, respectively) new reliable archaeodirectional data points from four different archaeological locations in this study. These are the first new directional data from China since the 1990s and fill many gaps of the present dataset in this area. The existing data from Eastern Asia generally agree with each other and fit well to the global models in the past 2 kyr reflecting the abundance of data for this period. However, at periods before 2 ka, data are sparse and supply few constraints for models, which make our new data, especially those from LJZ and DXZ, significant. The declinations and inclinations of the geomagnetic field in Eastern Asia vary between 30°W-20°E and 30°-70° respectively over the past 10 kyr. Both westward and eastward drift is observed and the former is generally dominant. Quite a few inflection points of the geomagnetic field direction are recorded in Eastern Asia over the past 10 kyr including those archaeomagnetic jerks reported in Europe (Gallet *et al.* 2003) and some of them are synchronous with the maxima (~4000 BCE, ~500 CE) and minima (~3000 BCE, ~100 BCE) of the paleointensity variations. The PSV rates of the field direction are generally low (according to present data distribution) before ~2000 BCE but are followed by fast increase and large fluctuations afterward, which is generally consistent with the pattern of paleointensity variations in this area.

ACKNOWLEDGMENTS

We thank Li Qin, Guangbiao Wei, Hao Dang, Zhenli Jiang, Jiqiao Guo, Sheng Huang, Shihu Li and Kunpeng Ge for assistance in sample collection. This work was funded by the NSFC grants 41504052 and 41274073, and the 973 program grant 2012CB821900. LT acknowledges support from NSF Grant No. EAR1520674 and EAR1345003. SC acknowledges further support from China Postdoctoral Science

Foundation. CD acknowledges further support from the CAS Bairen Program. XC acknowledges support from National Social Science Foundation of China (14BKG009). All the new data in this study are accessible from the MagIC database (http://earthref.org/MagIC/11189/).

REFERENCES

Ali, M., Oda, H., Hayashida, A., Takemura, K. & Torii, M., 1999. Holocene palaeomagnetic secular variation at Lake Biwa, central Japan, *Geophys. J. Int.,* **136,** 218-228.

Amit, H., Korte, M., Aubert, J., Constable, C. & Hulot, G., 2011. The time-dependence of intense archeomagnetic flux patches, *J. Geophys. Res.,* **116,** B12, doi: 10.1029/2011jb008538.

Aubert, J., Finlay, C.C. & Fournier, A., 2013. Bottom-up control of geomagnetic secular variation by the Earth's inner core, *Nature,* **502,** 219-223.

Banerjee, S.K., 1971. New grain size limits for palaeomagnetic stability in haematite, *Nature Physical Science*, **232**, 15-16.

Barletta, F., St-Onge, G., Channell, J.E.T. & Rochon, A., 2010. Dating of Holocene western Canadian Arctic sediments by matching paleomagnetic secular variation to a geomagnetic field model, *Quaternary Sci. Rev.,* **29,** 2315-2324.

Batt, C., Meng, Z. & NÖEl, M., 1998. New archaeomagnetic studies near Xi'an, China, *Archaeometry,* **40,** 169-175.

Ben-Yosef, E., Tauxe, L., Ron, H., Agnon, A., Avner, U., Najjar, M. & Levy, T.E., 2008b. A new approach for geomagnetic archaeointensity research: insights on ancient metallurgy in the Southern Levant, *J. Arch. Sci.*, **35**, 2863-2879.

Brown, M.C., Donadini, F., Korte, M., Nilsson, A., Korhonen, K., Lodge, A., Lengyel, S.N. & Constable, C.G., 2015. GEOMAGIA50.v3: 1. general structure and modifications to the archeological and volcanic database, *Earth Planets Space,* **67,** 1, doi: 10.1186/s40623-40015-40232-40620.

Brown, M.C. & Korte, M., 2016. A simple model for geomagnetic field excursions and inferences for palaeomagnetic observations, *Phys. Earth Planet. Inter.,* **254,** 1-11.

Cai, S., Chen, W., Tauxe, L., Deng, C., Qin, H., Pan, Y., Yi, L. & Zhu, R., 2015. New constraints on the variation of the geomagnetic field during the late Neolithic period: Archaeointensity results from Sichuan, southwestern China, *J. Geophys. Res. Solid Earth,* **120,** 2056-2069.

Cai, S., Tauxe, L., Deng, C., Pan, Y., Jin, G., Zheng, J., Xie, F., Qin, H. & Zhu, R., 2014. Geomagnetic intensity variations for the past 8 kyr: New archaeointensity results from Eastern China, *Earth Planet. Sci. Lett.,* **392,** 217-229.

Ertepinar, P., Langereis, C.G., Biggin, A.J., de Groot, L.V., Kulakoğlu, F., Omura, S. & Süel, A., 2016. Full vector archaeomagnetic records from Anatolia between 2400 and 1350 BCE: Implications for geomagnetic field models and the dating of fires in antiquity, *Earth Planet. Sci. Lett.,* **434,** 171-186.

Finlay, C.C., Maus, S., Beggan, C.D., Hamoudi, M., Lowes, F.J., Olsen, N. & Thébault, E., 2010. Evaluation of candidate geomagnetic field models for IGRF-11, *Earth Planets Space,* **20,** 1-19.

Fisher, R.A., 1953. Dispersion on a sphere, *Proc. R. Soc. Lon. Ser.-A,* **217,** 295–305.

Frank, U., 2007. Palaeomagnetic investigations on lake sediments from NE China: a new record of geomagnetic secular variations for the last 37 ka, *Geophys. J. Int.,* **169,** 29-40.

Gallet, Y., Genevey, A. & Courtillot, V., 2003. On the possible occurrence of 'archaeomagnetic jerks' in the geomagnetic field over the past three millennia, *Earth Planet. Sci. Lett.,* **214,** 237-242.

Hyodo, M., Yoshihara, A., Kashiwaya, K., Okimura, T., Masuzawa, T., Nomura, R., Tanaka, S., Tang, B.X., Liu, S.Q. & Liu, S.J., 1999. A late Holocene geomagnetic secular variation record from Erhai Lake, southwest China, *Geophys. J. Int.,* **136,** 784-790.

Jackson, A., Jonkers, A.R.T. & Walker, M.R., 2000. Four centuries of geomagnetic secular variation from historical records, *Philos. Trans.R. Soc. London A,* **358,** 957–990.

Jiang, Z., Liu, Q., Dekkers, M. J., Colombo, C., Yu, Y., Barrón, V. & Torrent, J., 2014. Ferro and antiferromagnetism of ultrafine- grained hematite, *Geochem. Geophys. Geosyst.*, **15,** 2699–2712, doi:10.1002/ 2014GC005377.

Kirschvink, J., 1980. The least-squares line and plane and the analysis of palaeomagnetic data, *Geophys. J. R. Astr. S.,* **62,** 699-718.

Korte, M. & Constable, C., 2011. Improving geomagnetic field reconstructions for 0–3ka, *Phys. Earth Planet. Inter.,* **188,** 247-259.

Korte, M., Constable, C., Donadini, F. & Holme, R., 2011. Reconstructing the Holocene geomagnetic field, *Earth Planet. Sci. Lett.,* **312,** 497-505.

Korte, M., Donadini, F. & Constable, C.G., 2009. Geomagnetic field for 0-3 ka: 2. A new series of time-varying global models, *Geochem. Geophys. Geosyst.,* **10,** Q06008, doi: 06010.01029/02008gc002297.

Nilsson, A., Holme, R., Korte, M., Suttie, N. & Hill, M., 2014. Reconstructing Holocene geomagnetic field variation: new methods, models and implications, *Geophys. J. Int.,* **198,** 229-248.

Noel, M. & Batt, C.M., 1990. A method for correcting geographically separated remanence directions for the purpose of archaeomagnetic dating, *Geophys. J. Int.,* **102,** 753-756.

Ólafsdóttir, S., Geirsdóttir, A., Miller, G.H., Stoner, J.S. & Channell, J.E.T., 2013. Synchronizing Holocene lacustrine and marine sediment records using paleomagnetic secular variation, *Geology,* **41,** 535-538.

Pavón-Carrasco, F.J., Rodríguez-González, J., Osete, M.L. & Torta, J.M., 2011. A Matlab tool for archaeomagnetic dating, *J. Arch. Sci.,* **38,** 408-419.

Shaar, R. & Tauxe, L., 2013. Thellier GUI: An integrated tool for analyzing paleointensity data from Thellier-type experiments, *Geochem. Geophys. Geosyst.,* **14,** 677-692.

Tarduno, J.A., Watkeys, M.K., Huffman, T.N., Cottrell, R.D., Blackman, E.G., Wendt, A., Scribner, C.A. & Wagner, C.L., 2015. Antiquity of the South Atlantic Anomaly and evidence for top-down control on the geodynamo, *Nat. Commun.,* **6,** 7865, doi: 7810.1038/ncomms8865.

Tauxe, L., Banerjee, S.K., Butler, R.F. & van der Voo, R., 2010. Essentials of Paleomagnetism, *Univ. of Calif. Press, Berkeley.***,** pp: 85–98.

Tauxe, L. & Staudigel, H., 2004. Strength of the geomagnetic field in the Cretaceous Normal

Superchron: New data from submarine basaltic glass of the Troodos Ophiolite, *Geochem. Geophys. Geosyst.,* **5,** Q02H06, doi: 10.1029/2003gc000635.

Wei, Q.Y., Li, D.J., Cao, G.Y., Zhang, W.X. & Wang, S.P., 1984. The wandering path of virtual geomagnetic pole during the last 6000 years, *Acta Geophysica Sinica,* **27,** 562-572.

Wei, Q.Y., Li, T.C., Chao, G.Y., Chang, W.S. & Wang, S.P., 1981. Secular variation of the direction of the ancient geomagnetic field for Loyang region, China, *Phys. Earth Planet. Inter.,* **25,** 107-112.

Wei, Q.Y., Li, T.C., Chao, G.Y., Wang, S.P. & Wei, S.F., 1983. Results from China, In: Creer K.M., Tucholka P., Barton C.E.; Geomagnetism of baked clays and recent sediments, *Elsevier:Amsterdam; 324,* pp**:** 138-150.

Yang, X., Heller, F., Yang, J. & Su, Z., 2009. Paleosecular variations since ~9000 yr BP as recorded by sediments from maar lake Shuangchiling, Hainan, South China, *Earth Planet. Sci. Lett.,* **288,** 1-9.

Yang, X., Liu, Q., Duan, Z., Su, Z., Wei, G., Jia, G., Ouyang, T., Su, Y. & Xie, L., 2012. A Holocene palaeomagnetic secular variation record from Huguangyan maar Lake, southern China, *Geophys. J. Int.,* **190,** 188-200.

Yang, X., Liu, Q., Yu, K., Huang, W., Zhu, L., Zhang, H., Liu, J. & Li, J., 2016. Paleosecular variations of the geomagnetic field during the Holocene from Eastern Asia, *Phys. Earth Planet. Inter.,* **254,** 25-36.

Yu, Y., Doh, S.-J., Kim, W., Park, Y.-H., Lee, H.-J., Yim, Y., Cho, S.-G., Oh, Y.-S., Lee, D.-S., Lee, H.-H., Gong, M.-G., Hyun, D.-H., Cho, J.-K., Sin, Y.-S. & Do, M.-S., 2010. Archeomagnetic secular variation from Korea: Implication for the occurrence of global archeomagnetic jerks, *Earth Planet. Sci. Lett.,* **294,** 173-181.

Zheng, Y., Zheng, H., Deng, C. & Liu, Q., 2014. Holocene paleomagnetic secular variation from East China Sea and a PSV stack of East Asia, *Phys. Earth Planet. Inter.,* **236,** 69-78.

Zijderveld, J.D.A., 1967. A.C. demagnetization of rocks: analysis of results. In: Collinson, D., Creer, K., Runcorn, S. (Eds.), *Methods in Paleomagnetism***,** pp: 254–286.

Table 1 Statistic results on sample and site level.

Sample/Site	Age	Dec	Inc	Dec-reloc	Inc-reloc	α_{95}(°)	κ	n_a/n_0	N_a	Lon	Lat	VGP-Lon	VGP-Lat
	(BCE/CE)	(°)								(°E)	(°N)	(°)	
BJY2		353.5	58.2			2.4	523.9	8/8					
BJY5		5.6	56.0			3.0	507.6	6/8					
Ave(BJY2-5)	**1320±49[a]**	**358.8**	**57.4**	**358.1**	**51.3**	**2.4**	**267.9**		**2**	**117.74**	**41.33**	**313.7**	**86.6**
DXZ1		347.4	56.9			5.4	155.1	6/9					
DXZ2*		355.4	59.5			17.2	13.3	7/7					
Ave(DXZ1)	**-1150±150[a]**	**347.4**	**56.9**	**348**	**57.3**	**5.4**	**155.1**		**1**	**117.11**	**36.71**	**35.3**	**79.9**
DXZ3		351.8	58.8			6.5	358.3	3/5					
DXZ5		345.3	65.7			7.9	135.6	4/7					
DXZ6		349.8	57.8			2.8	741.2	5/7					
DXZ7		333.4	59.0			5.7	178.3	5/7					
DXZ8		351.5	58.3			3.2	1475.6	3/5					
Ave(DXZ3-8)	**-1150±150[a]**	**345.4**	**60.1**	**347.1**	**60.7**	**2.6**	**152.8**		**5**	**117.11**	**36.71**	**52.3**	**77.9**
DXZ9		1.2	51.2			1.9	1062.2	7/7					
DXZ10		2.5	53.1			2.1	852.9	7/7					
DXZ11		5.0	52.8			1.4	2186.1	6/6					
Ave(DXZ9-11)	**-1150±150[a]**	**2.8**	**52.4**	**1.8**	**50.1**	**1.1**	**963.2**		**3**	**117.11**	**36.71**	**264.6**	**85.6**
DXZ14		359.7	50.0			4.7	166.9	7/7					
Ave(DXZ14)	**-1150±150[a]**	**359.7**	**50.0**	**358.3**	**48.3**	**4.7**	**166.9**		**1**	**117.11**	**36.71**	**299.6**	**84.1**
SWC1		356.0	52.3			7.1	167.4	4/11					
SWC2		348.8	47.2			3.5	297.7	7/12					
Ave(SWC1-2)	**1164±204[a]**	**351.3**	**49.1**	**349.7**	**48.8**	**3.4**	**178.1**		**2**	**118.70**	**37.14**	**346.6**	**79.8**

Y21*	-2893±27[b]	357.3	48.8			10.1	58.3	5/5					
Y3	**-2677±99[c]**	**8.1**	**48.1**	**8.6**	**52.1**	**2.9**	**273.5**	**10/10**	**1**	**101.53**	**31.80**	**210.4**	**82.5**
Y4	**-3011±95[c]**	**13.4**	**51.2**	**14.0**	**55.1**	**3.5**	**167.4**	**11/13**	**1**	**101.53**	**31.80**	**187.6**	**78.6**
Y5	**-3004±87[c]**	**15.4**	**43.6**	**16.3**	**48.3**	**6.8**	**97.9**	**6/6**	**1**	**101.53**	**31.80**	**212.8**	**75.1**
Y6	**-3011±95[b]**	**6.3**	**50.0**	**6.6**	**53.8**	**5.8**	**135.7**	**6/6**	**1**	**101.53**	**31.80**	**200.5**	**84.5**
Y7	**-3011±95[b]**	**4.7**	**51.3**	**4.9**	**54.9**	**4.8**	**69.4**	**14/14**	**1**	**101.53**	**31.80**	**187.9**	**86**
Y8	**-2725±98[c]**	**8.0**	**53.6**	**8.1**	**57.1**	**1.3**	**477.7**	**27/27**	**1**	**101.53**	**31.80**	**170.1**	**82.9**

Dating methods of the ages are marked with character notes, a: archaeological dating; b: stratigraphic information combining with ^{14}C dating; c: ^{14}C dating. Dec/Inc: declination/inclination; Dec-reloc/Inc-reloc: relocated declination/inclination; α_{95}: 95% confidence limit; κ: precision parameter; n_a/n_0: number of accepted/experiment specimens; N_a: number of accepted samples; Lon/Lat: Longitude/Latitude; VGP-Lon/VGP-Lat: Longitude/Latitude of VGP. Samples marked with '*' are rejected because of $\alpha_{95} \geq 10°$.

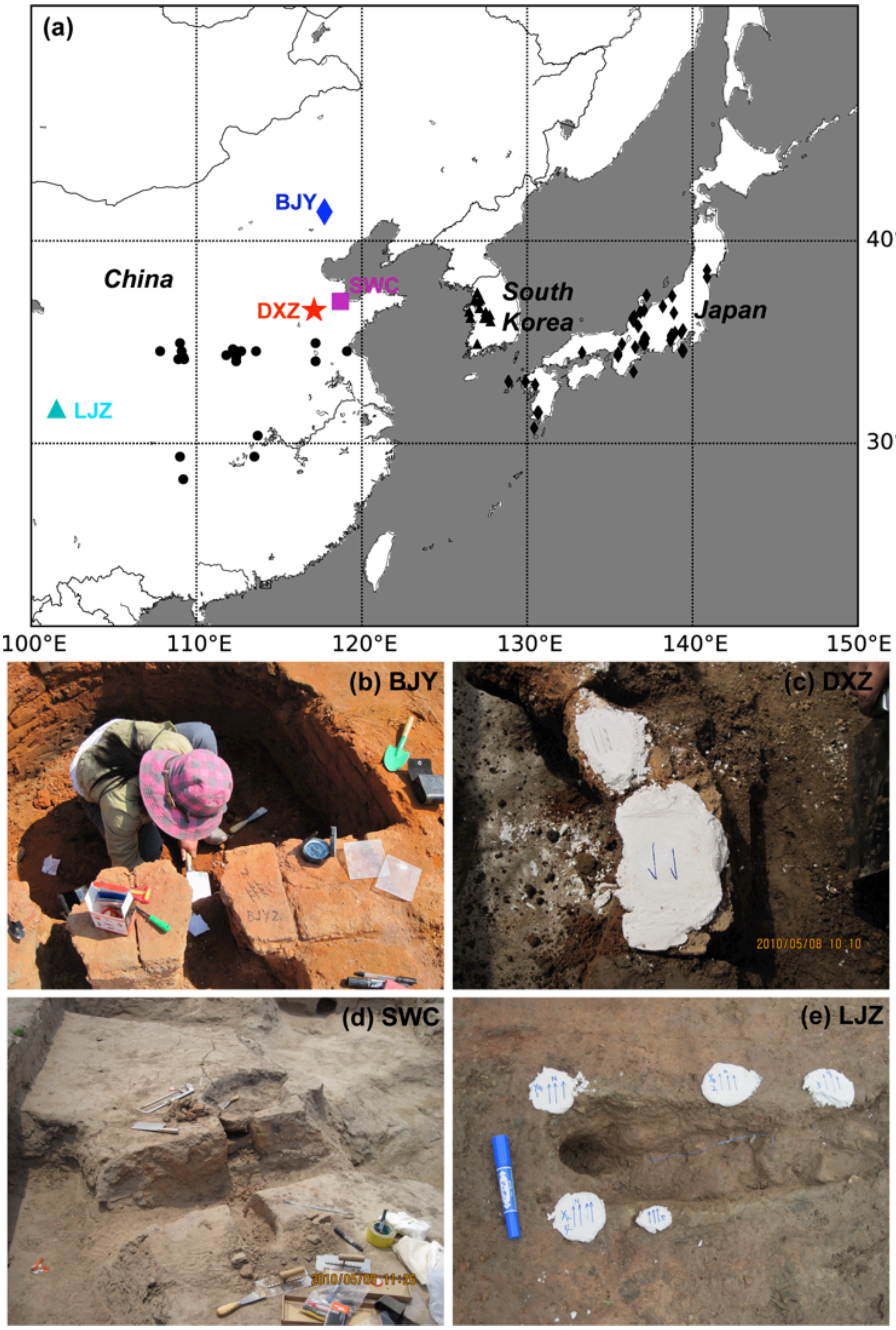

Fig. 1 (a) Sitemap of this study and the published data in Eastern Asia. Blue diamond/red star/purple square/cyan triangle is the locations of BJY/DXZ/SWC/LJZ in this study. Black solid circles/triangles/diamonds represent locations of the published directional data in China/Korea/Japan from the GEOMAGIA50 database after data selection. Data selection criteria please see the text. (b-e) Representative

pictures of the four sampling locations: (c) is the hearth of DXZ1; (d) is Y4 from LJZ.

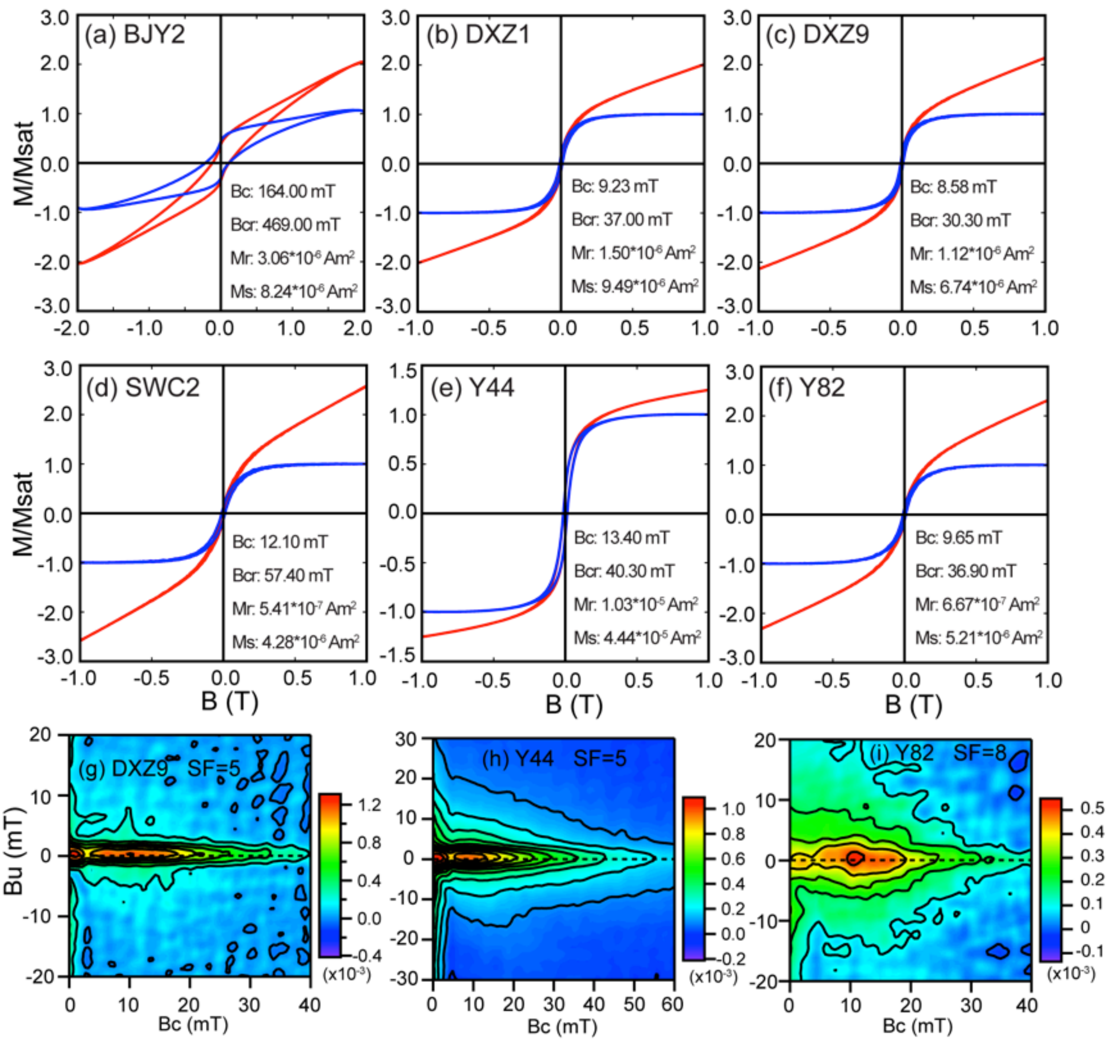

Fig. 2 (a-f) Hysteresis loops of representative samples. Red (blue) loop is before (after) paramagnetic correction. Bc, coercivity; Bcr, remanent coercivity; Mr, remanent magnetization; Ms, saturation magnetization. Data are analyzed with the software of Pmagpy-2.184. (g-i) FORC plots analyzed with the software of FORCinel_1.17.

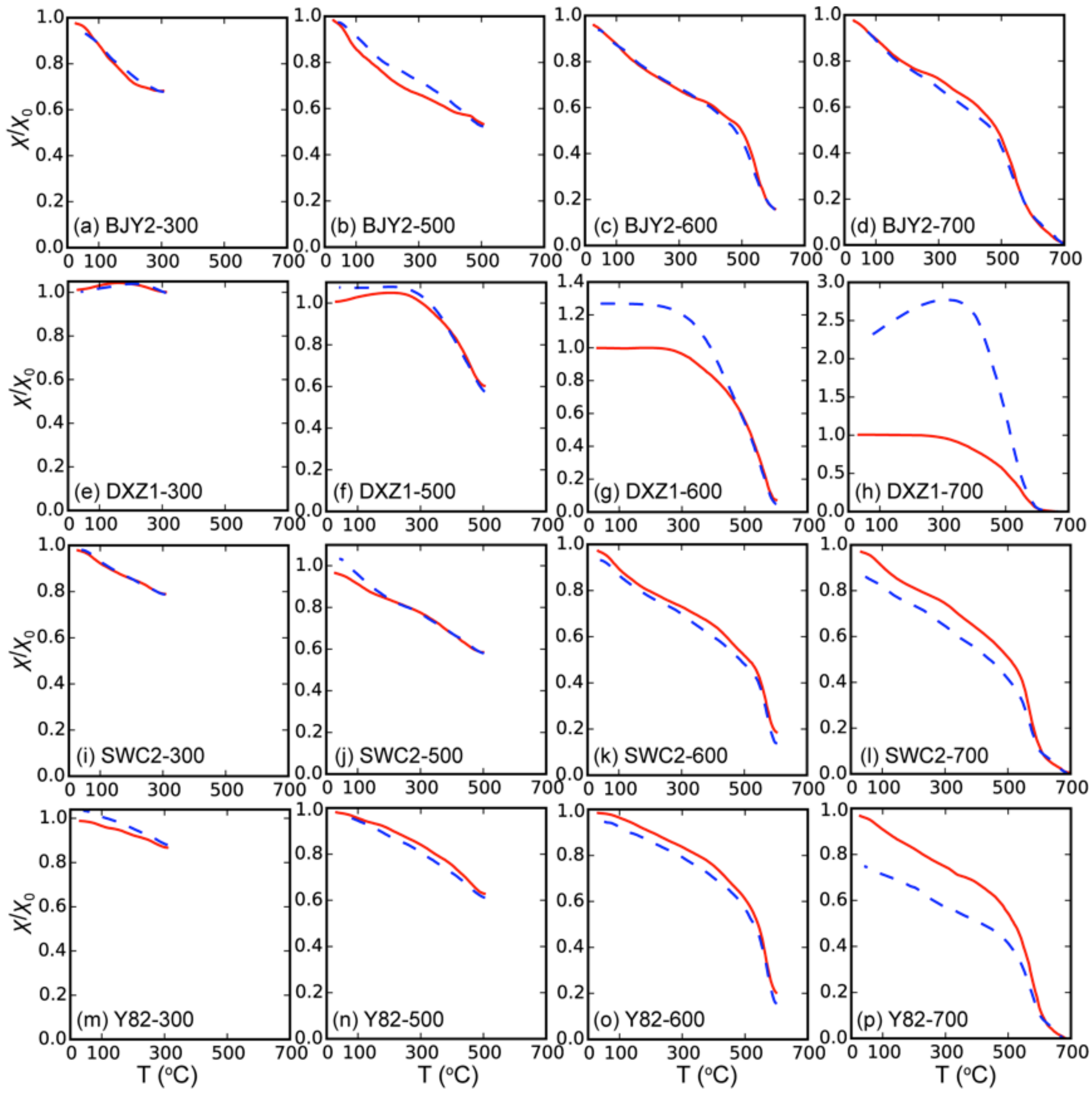

Fig. 3 Step-wise variations of normalized susceptibility versus temperature. Samples are processed in air. Red solid (blue dashed) line represents heating (cooling) procedure.

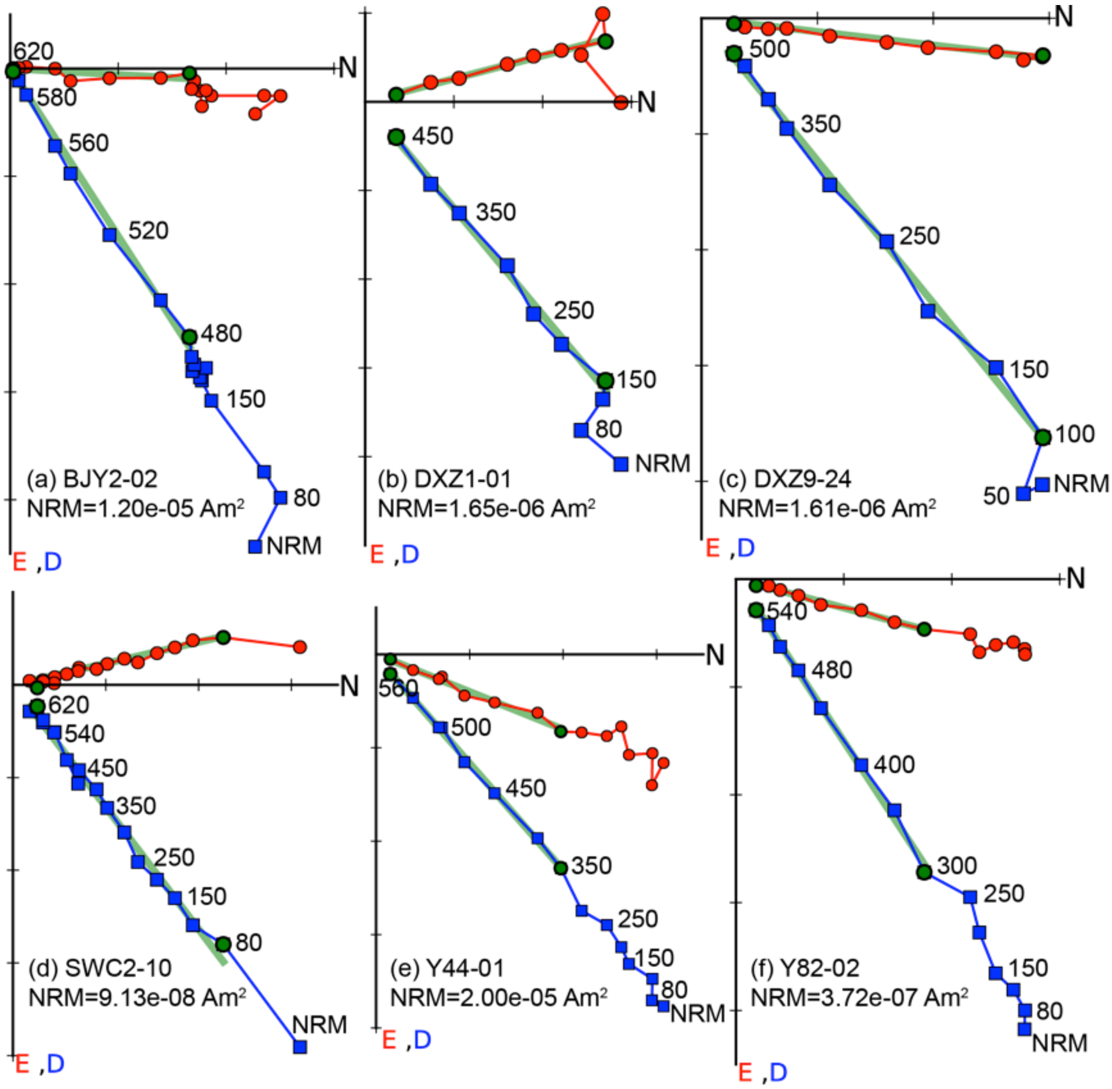

Fig. 4 Representative orthogonal projections for accepted specimens. Red solid circles/blue squares represent projections on horizontal/vertical plane. The green line on each plot shows the temperature section used to calculate the characteristic direction. Numbers on the diagrams are temperature steps in centigrade (°C). The plots were made with the software of Thellier_GUI (Shaar & Tauxe 2013).

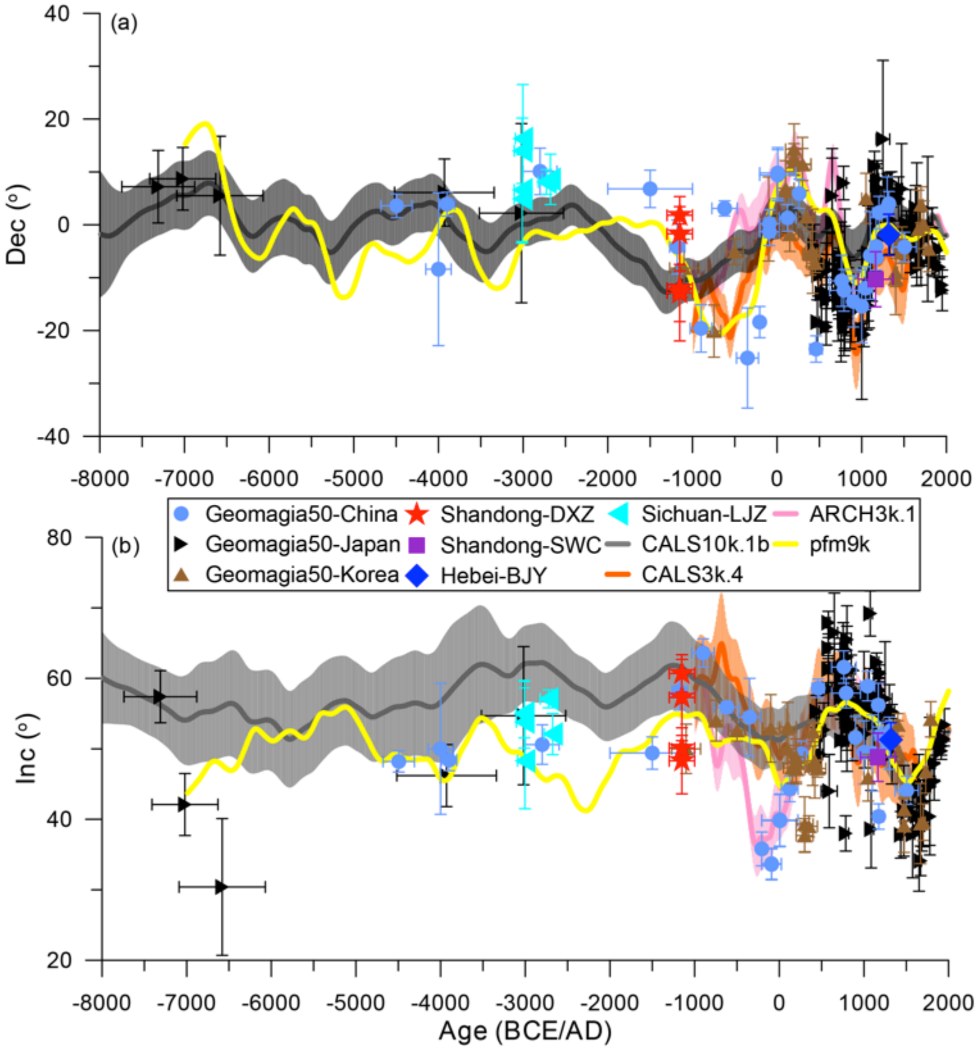

Fig. 5 Variations of geomagnetic declination (a) and inclination (b) versus age. Blue diamond/red stars/purple square/cyan left triangles are data from BJY/DXZ/SWC/LJZ in this study. Baby blue solid circles/brown triangles/black right triangles represent locations of the published directional data in China/Korea/Japan from the GEOMAGIA50 database after data selection. Error bars of declination and inclination are $\alpha_{95}/\cos I$ and α_{95} respectively. All the data in this figure are relocated to the center of China (35°N, 105°E). The grey/orange/pink/yellow line is the prediction from global model of CALS10k.1b/CALS3k.4/ARCH3k.1/pfm9k at the center of China (35°N, 105°E).

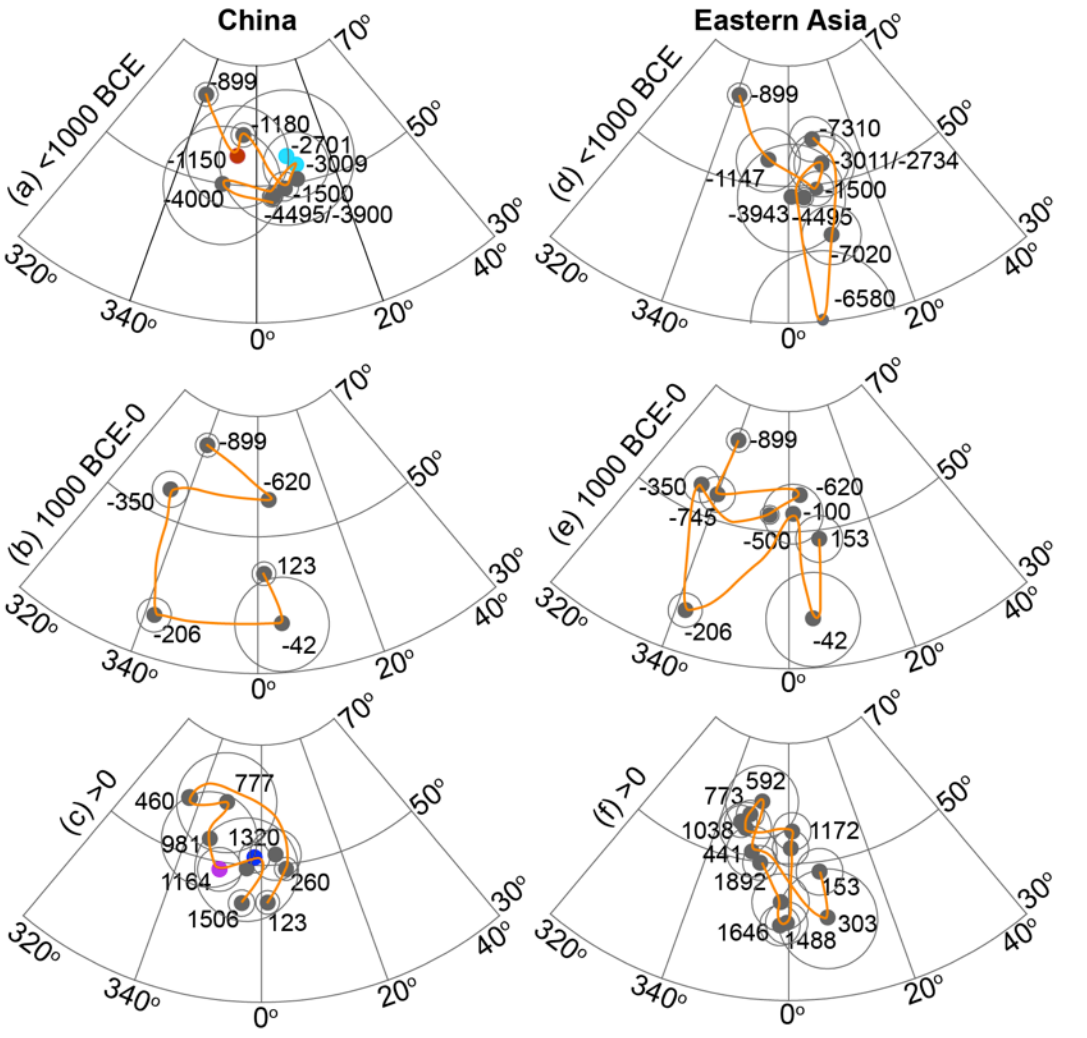

Fig. 6 D-I projections of the Chinese data (a-c) and all the Eastern Asian data (d-f). Fisher means of the data set in Fig. 5 are calculated with a time window of 100 years. The Fisher means of the new data in this study are marked with color dots in (a) and (c) (red/cyan/purple/blue: DXZ/LJZ/SWC/BJY). All the published and new data are included in the Eastern Asian projections. 95% confidence circles are shown for each data. Numbers in each plot are ages where negative represents 'BCE'. Orange lines show moving trajectories of the field.

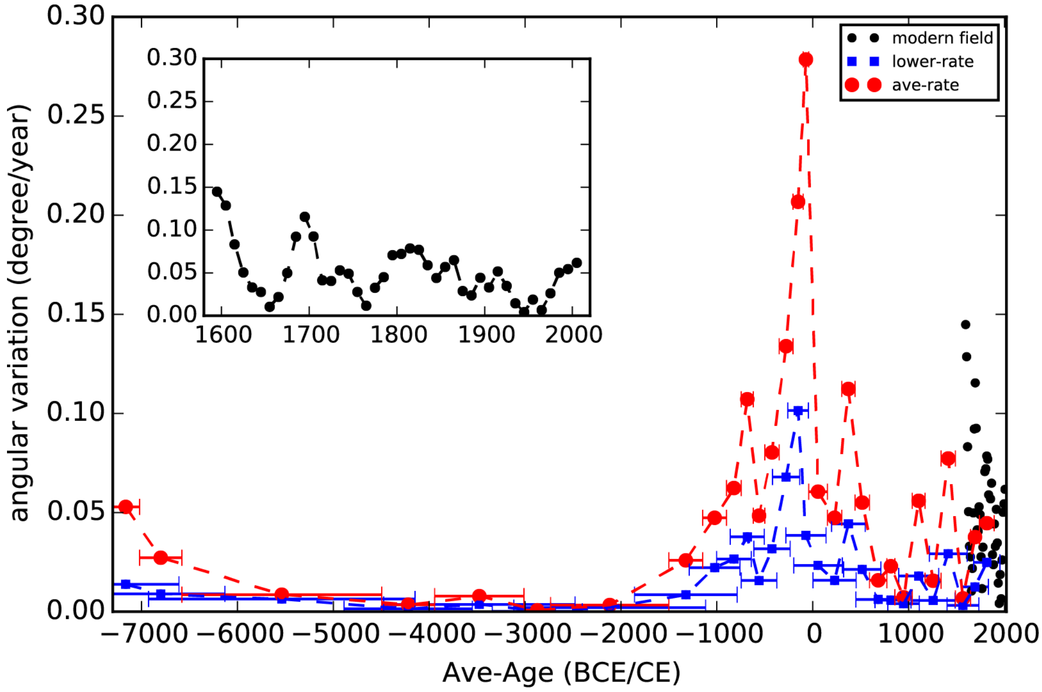

Fig. 7 PSV rate (angular variation per year) of the geomagnetic field in Eastern Asia over the past 10 kyr. Data from Fig. 6 are used for calculation. Ave-rate (red solid circle) is the average rate while lower-rate (blue square) is the lower boundary of the average rate. The age interval for each rate is shown with error bar on x axes. The insert is amplification of the variation rate of the modern field (black solid circle). The modern directions are predicted at the center of China (35°N, 105°E) by gufm1 model between 1590-1990 CE and IGRF model between 1990-2010 CE. PSV rates of the modern field are calculated at a 10-year window.

SUPPORTING INFORMATION

Table S1 The list of specimens passing selection criteria. T_{min}/T_{max}: minimum/maximum temperature step used to calculate the directions of ChRM. n: number of data points used for the calculation of ChRM directions. Dec/Inc: declination/inclination of each specimen. The declinations are corrected with local magnetic declinations of each area at the time of sampling. MAD: maximum angular deviation. DANG: deviation angle from the origin. Flag: a mark showing whether the specimen is accepted (‘g’) or excluded (‘b’).

Table S2 All the published data in Eastern Asia used in this study. N/n: number of samples/specimens, ‘-’ means unknown. The meanings of other items are the same as Table 1.

Specimen	T_{min} (°C)	T_{max} (°C)	n	Dec (°)	Inc (°)	MAD (°)	DANG (°)	Flag
BJY2-01	480	620	8	352.86	55.2	2.3	1.2	g
BJY2-02	480	620	8	355.86	56.7	2.8	1.1	g
BJY2-03	480	620	8	3.56	57.1	4	1.5	g
BJY2-04	480	620	8	358.66	59.5	3	0.7	g
BJY2-37	450	620	8	344.36	60.5	3.2	1.6	g
BJY2-38	450	560	5	351.56	58.8	3.5	1.4	g
BJY2-39	300	580	9	350.26	57.9	3.9	1.9	g
BJY2-40	450	580	6	349.66	58.9	2.6	0.3	g
BJY5-01	520	640	7	6.76	56.3	4.4	1.9	g
BJY5-02	500	640	8	180.86	68.8	4.7	3.5	b
BJY5-03	80	640	18	12.16	57.5	3.2	1.7	g
BJY5-04	580	640	4	186.76	59	1.5	1.5	b
BJY5-05	100	580	14	3.96	60.6	2.3	1.9	g
BJY5-06	540	640	5	4.66	54.2	2.1	0.3	g
BJY5-07	50	580	15	6.36	53.2	2.5	3	g
BJY5-08	560	640	5	0.16	53.6	1.9	0.5	g
DXZ1-01	150	450	7	339.82	49.2	2.2	0.3	g
DXZ1-04	100	450	8	342.72	57	1.7	1.9	g
DXZ1-05	100	450	8	337.42	57.6	2.1	3.7	g
DXZ1-38	100	500	9	3.92	58.3	2	1.2	g
DXZ1-39	50	500	10	351.42	58.1	2.1	1.7	g
DXZ1-40	100	500	9	351.52	59.2	1.5	0.9	g
DXZ2-01	100	480	9	325.72	53.4	1.5	2.1	g
DXZ2-02	300	480	5	39.92	29.4	3.3	3.7	g
DXZ2-03	300	450	4	13.02	51.2	5.6	3.8	g
DXZ2-04	150	480	8	343.22	61.3	4.5	3.6	g
DXZ2-05	80	500	11	343.02	52.9	5.1	2.1	g
DXZ2-06	80	500	11	306.52	72.6	4.6	2	g
DXZ2-07	200	480	7	347.02	70.5	4.7	3.2	g
DXZ3-03	250	500	7	347.32	35.1	4.5	2.2	b
DXZ3-04	80	480	10	349.62	60.4	4.4	1.5	g
DXZ3-05	150	500	9	345.72	57.1	5.3	5.8	g
DXZ3-06	150	450	7	0.32	58.6	2.3	2.7	g
DXZ4-17	100	560	12	4.42	65.2	4	5.6	g
DXZ4-21	350	580	8	327.32	-26.6	2.8	3	b
DXZ5-01	80	500	11	355.72	67.3	3.1	3.8	g
DXZ5-02	100	450	8	357.82	69.5	2.4	3.5	g
DXZ5-03	80	450	9	337.62	66.6	3.2	6	g
DXZ5-14	100	400	7	335.22	58.2	1.3	5.3	g
DXZ5-15	250	560	9	0.32	38.6	2.7	2.4	b
DXZ6-01	100	400	7	349.82	56.9	1.8	2.2	g
DXZ6-04	150	400	6	350.32	59.8	0.8	3.6	g
DXZ6-05	150	450	7	343.42	56	1.5	2.1	g
DXZ6-16	100	400	7	352.42	60.3	2.6	3.6	g
DXZ6-17	100	400	7	353.42	56	5.2	0.5	g
DXZ7-02	150	500	9	343.52	57.3	2.7	0.8	g

DXZ7-03	80	450	9	333.32	58.9	3.7	5.9	g
DXZ7-04	150	560	12	337.52	57.8	2.9	1.2	g
DXZ7-05	250	560	10	337.12	57.8	2.3	0.3	g
DXZ7-40	100	450	8	313.22	61	1.4	3.1	g
DXZ8-02	80	400	8	347.32	59.4	2.4	1.7	g
DXZ8-03	150	400	6	354.12	57.8	4.3	0.9	g
DXZ8-05	200	400	5	352.82	57.7	2.4	0.9	g
DXZ9-01	200	520	9	1.02	49.9	3	1.7	g
DXZ9-02	200	520	9	4.22	52.9	2.2	1.4	g
DXZ9-03	100	500	10	5.72	52.1	1.9	0.9	g
DXZ9-04	100	500	10	0.52	52.9	2.5	1.5	g
DXZ9-05	200	520	10	359.12	52	1.9	2.7	g
DXZ9-21	100	520	10	358.12	48	1.9	2.3	g
DXZ9-24	100	500	9	0.02	50.7	1.8	0.8	g
DXZ10-01	200	450	6	4.22	51.8	0.8	0.5	g
DXZ10-02	200	450	6	6.82	53	1.4	1.6	g
DXZ10-03	80	450	9	3.02	56.3	2.6	1.7	g
DXZ10-04	100	480	9	2.92	54.4	2.9	2	g
DXZ10-05	150	480	8	4.62	50.9	0.9	0.4	g
DXZ10-39	50	450	9	356.22	52.5	3.1	2.3	g
DXZ10-40	100	500	9	359.82	52.3	1.3	0.4	g
DXZ11-01	100	480	9	4.02	52.5	2.1	1.3	g
DXZ11-02	100	480	9	9.72	52.1	3	0.8	g
DXZ11-03	100	500	10	3.32	53.4	3	0.3	g
DXZ11-04	150	450	7	3.42	51.4	1.5	1	g
DXZ11-37	100	500	9	4.92	53.7	2.8	1.7	g
DXZ11-38	100	500	9	4.52	53.6	2.9	0.7	g
DXZ12-02	200	480	7	30.32	64.2	5.8	1.6	g
DXZ13-01	150	400	6	46.92	79.5	1.8	3.1	g
DXZ13-03	150	450	7	316.22	86.4	4.5	4.7	b
DXZ13-05	150	300	4	48.22	69	5.8	5.3	g
DXZ14-01	80	520	12	354.12	55.4	2.6	2.7	g
DXZ14-02	150	520	10	1.52	38.6	3.9	5	g
DXZ14-03	80	500	11	3.22	54.9	2.6	4	g
DXZ14-04	80	520	12	359.42	53.8	2.4	3.4	g
DXZ14-05	80	520	12	356.52	49.6	2.9	3.4	g
DXZ14-36	100	500	9	1.62	46.4	2.4	2.7	g
DXZ14-37	100	500	9	1.02	51.3	1.6	2.9	g
DXZ15-01	100	500	10	216.52	53.3	3	4.9	b
DXZ15-02	80	500	11	222.32	51.1	2.6	2.2	b
DXZ15-03	80	480	10	223.92	53.1	2.5	3.8	b
DXZ15-04	80	480	10	221.72	54.8	3.4	4.2	b
DXZ15-05	80	480	10	216.72	56.2	2.5	2.5	b
DXZ15-30	100	500	9	225.52	54.3	2.4	1.4	b
DXZ15-31	100	500	9	235.12	57.4	2.1	3	b
SWC1-21	100	580	13	347.04	55.2	5.2	5.2	g
SWC1-22	100	580	13	356.54	52.4	4.9	6	g
SWC1-42	80	640	18	351.04	50.1	4.9	3.3	g

SWC1-46	100	560	12	8.64	50.2	2.8	6	g
SWC2-09	200	640	15	350.44	44.7	5.4	5.1	g
SWC2-10	80	620	17	339.44	52.1	3.2	1.5	g
SWC2-11	80	520	12	346.34	51.6	4.8	0.9	g
SWC2-13	80	540	13	350.74	48.1	4.4	4.3	g
SWC2-15	50	580	14	354.04	45.3	3.5	3.7	g
SWC2-16	50	600	15	349.84	45.7	3.4	2.3	g
SWC2-21	50	540	12	349.34	42.7	2.3	2.5	g
SWC3-22	100	500	9	19.64	49.1	2	4.6	g
SWC3-24	400	580	7	57.84	-17.1	3.8	2.3	b
SWC3-36	350	500	4	22.14	-5.9	2.4	0.4	b
SWC3-41	100	480	9	38.04	42.8	1.9	2.5	g
SWC3-42	350	500	5	69.14	-39.6	2.6	4	b
Y21-11	200	480	7	3.18	46.1	2.6	0.6	g
Y21-12	350	480	4	5.48	45.3	2.9	4.2	g
Y21-13	250	520	8	12.38	52.5	2.9	1.2	g
Y21-14	250	480	6	344.68	41.5	1.7	0.8	g
Y21-15	150	520	10	340.38	55.3	2.4	3.4	g
Y31-14	400	500	4	358.38	39.2	2	4.6	g
Y32-01	200	560	11	11.38	50.2	1.1	1	g
Y32-02	400	560	7	6.78	46.2	2.1	1	g
Y32-03	300	560	9	1.58	46.4	3.3	0.4	g
Y32-04	300	560	11	10.08	47.1	4	1.2	g
Y32-05	400	560	7	8.88	42.3	4.1	2.7	g
Y32-06	200	560	11	4.58	46.8	2.3	0.4	g
Y32-07	200	560	11	5.68	44.9	2.1	0.8	g
Y32-08	350	560	10	7.58	46.4	1.7	0.2	g
Y33-01	480	580	6	14.18	54	2.7	1.4	g
Y33-02	300	580	10	11.88	56.2	3.9	0.5	g
Y42-01	400	540	6	22.18	50.2	4.5	4.5	g
Y42-02	300	540	8	1.98	50.1	2.1	1.4	g
Y42-03	300	540	8	359.88	42.4	1.2	1	g
Y43-01	350	560	8	17.28	52.4	2.6	1.4	g
Y43-02	300	560	9	19.28	52.7	2.9	2.2	g
Y44-01	350	560	8	20.38	46.7	2.3	0.6	g
Y44-02	350	560	8	17.58	51.4	2.6	0.8	g
Y44-03	350	520	7	13.38	56.4	2.8	2.1	g
Y44-04	350	520	7	16.68	49	1.5	0.1	g
Y45-01	450	560	6	8.98	53.3	1.6	1.1	g
Y45-02	400	560	7	11.08	56.2	1.4	1	g
Y46-01	120	540	12	335.98	17.8	4.9	4.1	b
Y51-01	300	520	7	15.58	50.5	3.6	1.2	g
Y51-02	350	540	7	9.38	47.7	1.5	0.2	g
Y52-01	300	540	8	11.08	42	4.5	1.5	g
Y53-03	350	540	7	6.78	43.8	1.3	1.2	g
Y53-04	300	540	8	16.78	37.8	1.2	0.5	g
Y53-05	300	540	8	30.88	38	3.7	0.6	g
Y61-01	150	540	11	12.48	55.4	2.8	0.7	g

Y61-02	200	540	10	14.98	50.1	1.9	0.4	g
Y62-01	80	560	14	353.88	43.3	3.8	6	g
Y62-02	200	540	10	4.18	45.8	2.9	1.3	g
Y62-03	80	500	11	3.88	49.4	5.7	4.4	g
Y62-04	150	500	9	11.28	54.4	3	2	g
Y72-01	80	540	14	320.98	49.4	4.4	5.3	g
Y72-02	250	540	9	1.78	48.6	3.5	2.9	g
Y72-03	200	560	11	354.38	50.7	3.3	1.6	g
Y72-04	250	560	10	348.68	51.5	4.5	4.7	g
Y73-01	200	520	9	12.98	51.5	2.3	1.1	g
Y73-02	150	480	8	14.68	53.5	2	1.9	g
Y73-03	150	500	9	15.18	53.6	3.6	3.1	g
Y73-04	150	520	10	12.48	48.7	3.4	2.4	g
Y73-05	150	520	10	15.58	49.7	4.2	3.3	g
Y73-06	80	540	13	3.48	48.7	5.9	3.7	g
Y73-07	80	600	16	4.88	48.7	5	3.3	g
Y73-08	80	480	10	14.08	51.3	1.6	4.8	g
Y73-09	150	560	12	4.98	50.9	4.1	0.2	g
Y73-10	150	540	11	18.38	48	2.9	3.7	g
Y81-01	80	540	13	359.58	52.5	3	1.5	g
Y81-02	120	540	12	5.98	52.1	2.1	1.4	g
Y81-03	120	540	12	4.68	50.9	1.5	0.9	g
Y81-04	120	520	11	7.28	51.7	3.3	0.6	g
Y81-05	120	520	11	7.08	48.2	3	0.8	g
Y81-06	200	520	9	7.88	51.5	1.5	0.6	g
Y81-07	250	520	9	6.18	51.2	1.7	0.6	g
Y81-08	350	560	8	9.38	49.5	2.4	0.5	g
Y81-09	200	520	9	10.98	50.9	3.6	0.7	g
Y81-10	120	520	11	3.88	54.4	2.2	0.3	g
Y81-11	120	560	13	355.58	51.9	3.5	2.8	g
Y81-12	120	520	11	3.98	51.6	1.6	0.7	g
Y82-01	80	500	11	7.48	55	2.8	1.8	g
Y82-02	300	540	8	13.48	55.9	1.6	0.5	g
Y82-03	200	520	9	8.18	52.1	1.7	1.1	g
Y82-04	150	520	10	9.88	56.5	1.4	0.4	g
Y82-05	150	520	10	6.18	53.4	1.4	0.6	g
Y82-06	120	480	9	10.88	56	1.7	2.7	g
Y82-07	250	480	6	12.98	54.5	2.3	0.5	g
Y82-08	120	520	11	8.08	53.5	2.8	0.9	g
Y82-09	80	500	11	7.08	58.3	3.1	4	g
Y82-10	150	500	9	14.48	55.3	2.9	0.2	g
Y82-11	250	500	7	8.18	56.3	1.8	1	g
Y82-12	80	450	9	11.68	57.1	1.9	4.7	g
Y82-13	250	500	7	15.88	53.5	4.5	4.4	g
Y82-14	80	480	10	5.38	54.8	3.3	3.2	g
Y82-15	150	480	8	16.18	56.4	4.3	4.8	g

Age	σ_{Age}	N	n	Dec	Inc	Dec-reloc	Inc-reloc	α_{95}	Lat/°E	Lon/°N
China										
-4495	185	-	-	4.4	48	3.6	48.2	1.5	34.4	112.4
-4000	150	-	-	352.1	48.7	351.6	50	9.3	34.3	108.9
-3900	90	-	-	4.4	48	3.9	48.4	1.5	34.4	109.2
-2800	200	-	-	10.2	46.9	10.1	50.6	2.8	30.4	113.7
-1500	500	-	-	7.4	49.7	6.8	49.4	2.3	34.5	112.4
-1180	90	-	-	355.3	57.3	355.8	58.2	2.7	34.5	111.8
-899	128	-	-	338.8	60	340.4	63.6	2	34.2	117.2
-620	150	-	-	3	56.2	3.1	55.9	0.8	35.1	109
-350	130	-	-	336.6	46.6	334.8	54.5	5.5	30.4	113.7
-206	10	-	-	343	33.2	341.6	35.8	2.4	34.3	109.25
-91	115	-	8	1	33.2	358.7	33.7	2.2	34.7	112.7
-91	115	-	-	1	33.2	0.2	33.6	2.2	34.7	107.8
7	213	-	5	11.4	41.1	9.4	39.8	3.7	34.7	113.6
7	213	-	-	11.4	41.1	9.8	39.9	3.7	34.8	112.2
123	98	-	-	2.6	44.1	1.3	44.3	1.8	34.7	112.4
260	40	-	-	6.3	49.4	5.9	49.3	1.8	34.7	109.1
460	74	-	-	336.6	53.9	336.5	58.6	1.3	34.7	119.1
763	145	-	-	349	61	349.4	61.6	2.3	34.7	107.8
790	170	-	-	347.4	57.3	347.6	57.9	2.1	35.1	109
900	50	-	-	345.8	50.8	345.5	51.6	3	35.1	109
1000	50	-	-	345	48.6	344.6	49.5	4.5	35.1	109
1044	84	-	-	347.6	57	348	58.9	2.1	34.2	112.4
1100	50	-	-	354.6	49.2	354.2	49.4	5.4	35.1	109
1170	60	-	-	355.7	56.1	355.9	56.2	3.1	35.1	109
1175	60	-	-	356.7	39.4	353.8	40.4	1.8	35.1	117.2
1203	76	-	-	2.4	45.5	2.3	51.9	1.9	29.3	109
1300	50	-	-	3.5	51.1	3.2	50.8	3.7	35.1	109
1320	49	-	-	3.9	45	4	52.6	1.4	28.1	109.2
1506	138	-	-	357.5	35.7	355.8	44.1	2	29.3	113.5
Japan										
-7310	430	1	6	3.9	60.1	7.2	57.4	3.7	35.24	138.66
-7020	390	1	5	14.4	48.9	8.7	42.1	4.4	34.72	139.36
-6580	510	1	5	15.9	39.2	5.5	30.4	9.7	35.61	138.94
-3930	588	1	4	10.2	52.7	6.1	46.2	4.4	36.9	138.2
-3020	497	1	3	1.7	57.4	2.2	54.7	9.8	36.9	138.2
440	30	21	-	356	53	356	55.3	2.3	34.48	135.5
475	25	6	-	346	42.7	341.6	51.8	2.6	34.47	135.5
485	25	29	-	354.6	44.6	350.5	49.2	2.6	34.47	135.5
525	25	12	-	350.5	49.9	347	52.7	3.8	38.3	140.88
580	40	20	-	349.1	57.2	352.6	61.3	1.9	34.47	135.5
580	40	10	-	346.8	52.3	347.1	58.5	3.8	34.47	135.5
580	20	9	-	337.1	57.3	340.7	64.3	1.5	36.32	136.37
580	20	9	-	337.2	62.4	345.8	67.9	1.6	36.32	136.37
590	95	7	-	358.5	41.7	351.4	44	5.2	35.75	139.42
650	40	13	-	350.1	64.5	0.4	66.5	5.6	34.47	135.5
650	40	21	-	359.4	61.9	5.5	61.5	3.4	34.48	135.48

720	20	14	-	344.4	55.3	346.8	61.5	4.2	34.6	135.5
725	25	11	-	344.4	53.9	344.9	59.1	1	36.62	136.85
725	25	13	-	350.6	55.8	351.7	58.1	1.5	36.7	137.07
725	25	13	-	349.9	54.4	350.2	57.3	2.5	36.7	137.07
730	20	5	-	348.4	55.1	350.4	60	4.1	34.48	135.5
730	20	13	-	356.7	48.3	354	51.2	3	34.5	135.48
755	45	9	-	344.8	55.5	347.3	61.6	6.3	34.5	135.5
775	25	11	-	349.6	51.7	349.2	56.7	1.9	34.9	136.53
775	25	9	-	349.9	50.5	348.8	55.7	2	34.9	136.53
775	25	9	-	347.6	52.6	347.9	58.2	2.2	34.9	136.53
775	25	13	-	343.2	56.5	346.2	61.8	3.2	36.58	138.87
785	35	14	-	343.9	51.1	341.8	56.5	1.2	38.62	140.88
785	35	14	-	345.7	51.2	343.4	55.7	2	38.62	140.88
785	35	14	-	16.2	50.2	7.9	38	2.5	38.62	140.88
790	20	16	-	337.1	57.2	340.7	64	2.4	37.4	138.77
790	10	23	-	346.6	49.5	345.1	56	1.4	35.05	135.73
790	10	9	-	349.6	48.3	347.2	53.9	2.2	35.05	135.73
800	50	8	-	349	58.5	353.3	63	4.4	33.02	130.48
800	50	10	-	343.1	59.5	348.2	65.5	4.8	33.02	130.48
800	20	14	-	347.3	45.4	343.6	53	3.2	35.08	137.02
800	20	11	-	347.8	43.2	343	51.1	4.3	35.12	137.07
815	35	14	-	346.1	47.5	344.2	56.1	2.9	33.67	136.43
815	15	17	-	345.6	50.8	344.9	57.6	2.1	35.12	137.08
825	25	17	-	349.5	47.2	346.1	53.2	2.3	35.62	139.32
838	0	7	-	347.6	49.7	346.4	56.8	3	34.69	139.44
850	50	15	-	347.1	50.9	346.2	56.9	1.7	35.37	137.08
850	50	18	-	346.6	56.6	349.7	61.3	2	35.37	137.08
864	0	7	-	348.4	46.5	344.9	53.3	5	35.48	138.7
875	25	10	-	344.3	50.7	343.5	58.1	3	35.62	139.32
990	10	13	-	345.5	50.7	344.6	57.4	1.8	35.37	137.08
1000	20	9	-	342.6	47.5	340.2	56.5	7.3	35.1	137
1010	10	11	-	350.7	46.7	347.3	52.1	4.8	35.37	137.08
1025	25	9	-	341.1	48.3	339.2	57.7	1.2	35.12	137.1
1030	10	19	-	349.1	51.5	348.4	56.5	1.9	35.37	137.08
1050	10	15	-	349.6	50.8	348.4	55.7	0.9	35.37	137.08
1062	12	10	-	346	52	346	58.3	3.1	35.12	137.12
1075	25	14	-	341.9	65.2	354.6	69.2	3.2	35.07	137.07
1075	25	10	-	346.5	49.4	344.7	56.3	1.6	35.62	139.32
1085	30	8	-	357.4	32.5	347.5	38.6	5.5	34.69	139.4
1120	20	10	-	355.7	51.2	354.3	53.6	5.2	35.1	137
1150	25	11	-	2.9	65.2	11.1	62.3	1.3	35.37	137.08
1162	12	12	-	357	55.9	358.3	56.8	3.9	35.15	136.98
1175	25	20	-	357.4	58.7	0.2	58.4	1.6	35.93	136.72
1175	25	19	-	6.9	59.8	8.7	55.6	1.6	35.93	136.72
1175	25	14	-	3.4	61.2	7.1	58.2	1.9	35.93	136.72
1175	25	12	-	359.5	58.6	1.8	57.4	2.6	35.93	136.72
1187	12	12	-	0	54.9	0.1	54.6	0.9	35.37	137.08
1187	12	11	-	358.4	61.4	3.8	60.7	1.2	35.37	137.08

1187	12	13	-	2.3	58.8	4.8	57	4	35.37	137.08
1250	80	7	-	12.4	63.1	16.2	57.1	8.1	35.2	137.1
1300	20	12	-	2.1	57.1	3.3	55.5	3.6	35.37	137.08
1330	30	14	-	6.5	58.9	8.2	55.3	1	35.37	137.08
1330	10	8	-	4	50.5	1	49.3	4.3	34.75	139.35
1350	50	40	-	6.9	58.5	6.7	53.1	2	37.43	137.22
1435	15	15	-	12.8	43.4	4.9	37.8	3.3	34.69	139.41
1471	10	1	5	11.4	41.4	6.8	41.2	6.43	31.6	130.7
1525	25	19	-	6.6	43.6	359.9	41.1	1.4	35.3	137.15
1530	0	16	-	6.6	44.2	0.1	41.7	1.9	35.35	137.17
1575	25	5	-	7.4	39.7	358.8	37.9	6.2	34.77	139.43
1625	25	14	-	7.1	42.9	0.2	40.5	1.7	35.07	137.12
1635	35	19	-	8	49.3	3.2	44.8	3	36.2	136.42
1650	50	17	-	359.4	40.2	354.8	43.9	2.1	33.18	128.87
1650	50	16	-	355.7	41.9	351.8	46.9	2.3	33.18	128.87
1651	0	10	-	8.6	41.4	0.9	38.3	8.5	35.07	137.12
1670	10	23	-	6.1	34.8	357.8	34.1	2.1	34.63	133.32
1684	0	7	-	5.4	40.1	357.3	39.5	4	34.74	139.43
1700	10	13	-	359	39.7	352.8	42.5	3.1	34.63	133.32
1700	25	10	-	5.6	42.9	358.4	40	3.9	36.2	136.42
1777	0	15	-	5.3	41	357.6	40.4	4.1	34.73	139.41
1779	10	1	3	3.36	40.9	359.2	44.7	9.76	31.6	130.7
1830	10	11	-	358.4	47.3	354	47.9	2.3	36.2	136.42
1830	10	20	-	4.3	48.1	359.4	45.4	2.7	36.4	136.48
1860	20	36	-	355.4	46.2	352.9	50.8	1.7	33.18	129.9
1914	1	-	#	354.9	43.4	352	50.4	1.3	31.6	130.62
1914	1	-	#	358.2	44.2	355.4	49.7	1.2	31.57	130.62
1946	1	-	#	351.6	43	348.6	51.4	1	31.58	130.69
1950	0	8	-	350.6	47	347.6	53.4	2.3	34.73	139.38
Korea										
-1100	170	-	#	354.1	49.4	351.8	50	3.5	36.64	126.49
-745	80	-	#	341.7	49.5	339.9	54	2.9	36.64	126.49
-500	100	-	#	356	52.5	354.9	52.6	1.5	36.34	126.57
-100	100	-	8	1.7	55.6	1.1	52.9	4.8	37.24	127.17
100	100	-	#	8.6	54.2	6.9	50	2	36.64	126.49
100	100	-	#	6.7	56.5	6.3	53.1	3.5	36.33	127.4
150	100	-	#	1.1	50.2	358.2	47.3	2.2	37.56	126.98
200	100	-	#	15.4	53.8	12.7	47.1	1.8	36.63	127.49
200	100	-	#	13.8	54.6	11.9	48.8	1.7	36.33	127.4
200	100	-	#	16.6	55.2	14.3	48.2	3.2	36.81	127.11
300	100	-	#	16.5	47.2	11.5	39.3	3.9	36.81	127.11
300	100	-	#	16.9	46.4	11.4	37.7	2.4	37.24	127.17
350	100	-	#	6.8	43.7	1.5	39	1.5	37.15	127.07
395	75	-	#	357.6	48.1	354.6	47.6	2.8	36.64	126.49
400	100	-	#	355.6	52.6	354.4	52.4	1.4	36.81	127.11
420	80	-	6	357.7	49.5	355	48.3	5.3	37.2	126.83
450	100	-	#	355.9	47.7	352.7	47.2	1.2	37.2	126.83
1050	50	-	#	8.1	50.2	5	45.9	3.3	36.64	126.49

1400	20	-	#	352.2	50.6	351	53.4	1.6	35.06	126.98
1400	20	-	#	352.5	46.4	349.8	49.6	4.4	35.06	126.98
1475	25	-	#	0.4	40	354.7	39.1	3.8	36.49	127.73
1475	25	-	#	0	42.4	355	41.4	1.7	36.49	127.73
1670	25	-	8	4.6	41.8	359.2	39.4	5.7	36.17	127.78
1700	25	-	#	9	43.9	3.8	39.6	2.6	36.17	127.78
1730	25	-	#	3.1	48.7	0	46.8	3.1	36.17	127.78
1790	40	-	#	355.7	54.5	355.4	54.2	2.5	36.64	126.49